

Nonnegative Low Rank Tensor Approximation and its Application to Multi-dimensional Images

Tai-Xiang Jiang* Michael K. Ng[†] Junjun Pan[‡] Guang-Jing Song[§]

November 10, 2021

Abstract

The main aim of this paper is to develop a new algorithm for computing Nonnegative Low Rank Tensor (NLRT) approximation for nonnegative tensors that arise in many multi-dimensional imaging applications. Nonnegativity is one of the important property as each pixel value refer to nonzero light intensity in image data acquisition. Our approach is different from classical nonnegative tensor factorization (NTF) which has been studied for many years. For a given nonnegative tensor, the classical NTF approach is to determine nonnegative low rank tensor by computing factor matrices or tensors (for example, CPD finds factor matrices while Tucker decomposition finds core tensor and factor matrices), such that the distance between this nonnegative low rank tensor and given tensor is as small as possible. The proposed NLRT approach is different from the classical NTF. It determines a nonnegative low rank tensor without using decompositions or factorization methods. The minimized distance by the proposed NLRT method can be smaller than that by the NTF method, and it implies that the proposed NLRT method can obtain a better low rank tensor approximation. The proposed NLRT approximation algorithm is derived by using the alternating averaged projection on the product of low rank matrix manifolds and non-negativity property. We show the convergence of the alternating projection algorithm. Experimental results for synthetic data and multi-dimensional images are presented to demonstrate the performance of the proposed NLRT method is better than that of existing NTF methods.

Keywords: Nonnegative matrix, nonnegative tensor, low rank approximation, nonnegative matrix factorization, manifolds, projections, classification

AMS subject classifications. 15A23, 65F22.

*FinTech Innovation Center, Financial Intelligence and Financial Engineering Research Key Laboratory of Sichuan province, School of Economic Information Engineering, Southwestern University of Finance and Economics, Chengdu (email: taixiangjiang@gmail.com). T.-X. Jiang's research is supported in part by the Fundamental Research Funds for the Central Universities (JBK2001011).

[†]Department of Mathematics, The University of Hong Kong, Pokfulam, Hong Kong. (email: mng@maths.hku.hk). M. Ng's research is supported in part by the HKRGC GRF 12306616, 12200317, 12300218, 12300519 and 17201020.

[‡]Department of Mathematics and Operational Research, Faculté Polytechnique, Université de Mons, Belgium. (email: junjun.pan@umons.ac.be)

[§]School of Mathematics and Information Sciences, Weifang University, Weifang 261061, P.R. China. (email: sgjshu@163.com)

1 Introduction

Nonnegative data matrices appear in many data analysis applications. For instance, in image analysis, image pixel values are nonnegative and the associated nonnegative image data matrices can be formed for clustering and recognition [1–12]. In text mining, the frequencies of terms in documents are nonnegative and the resulted nonnegative term-to-document data matrices can be constructed for clustering [13–16]. In bioinformatics, nonnegative gene expression values are studied and nonnegative gene expression data matrices are generated for diseases and genes classification [17–21]. Low rank matrix approximation for nonnegative matrices plays a key role in all these applications. Its main purpose is to identify a latent feature space for objects representation. The classification, clustering or recognition analysis can be done by using these latent features.

Nonnegative Matrix Factorization (NMF) has emerged in 1994 by Paatero and Tapper [22] for performing environmental data analysis. The purpose of NMF is to decompose an input m -by- n nonnegative matrix $\mathbf{A} \in \mathbb{R}_+^{m \times n}$ into m -by- r nonnegative matrix $\mathbf{B} \in \mathbb{R}_+^{m \times r}$ and r -by- n nonnegative matrix $\mathbf{C} \in \mathbb{R}_+^{r \times n}$: $\mathbf{A} \approx \mathbf{BC}$, and more precisely

$$\min_{\mathbf{B}, \mathbf{C} \geq 0} \|\mathbf{A} - \mathbf{BC}\|_F^2, \quad (1)$$

where $\mathbf{B}, \mathbf{C} \geq 0$ means that each entry of \mathbf{B} and \mathbf{C} is nonnegative, $\|\cdot\|_F$ is the Frobenius norm of a matrix, and r (the low rank value) is smaller than m and n . Several researchers have proposed and developed algorithms for determining such nonnegative matrix factorization in the literature [1, 8, 23–32]. Lee and Seung [1] proposed and developed NMF algorithms, and demonstrated that NMF has part-based representation which can be used for intuitive perception interpretation. For the development of NMF, we refer to the recently edited book [33].

Nowadays, data that comes from many fields are more naturally represented as multi-dimensional data which refers to as tensor, for example, video data, hyperspectral data, fMRI data and so on. For more details and applications, we refer to the review paper [34]. To handle tensor data, there are two well-known and widely used decompositions, Canonical Polyadic decomposition (CPD) and Tucker decomposition. Because of the interpretability of NMF, many nonnegative tensor decompositions or models are proposed and developed. Most models are focused on CPD and Tucker decomposition with the nonnegative constraints.

For the CPD with nonnegative constraints, which is known as Nonnegative Tensor Factorization (NTF), early in 2001, Max Welling et.al, introduced a fixed point algorithm in [35]. Cichocki et al. [26, 36] developed a class of optimized local algorithms known as Hierarchical ALS (HALS), also extended the approach to other cost functions using the Alpha and Beta divergences for NTF computation. In [37], Park et al. proposed an NTF algorithm based on the alternating nonnegative constrained least squares method. In [38], the block principal pivoting method is further introduced to solve nonnegative constrained least squares (NNLS) to overcome some difficulties for the NNLS problems with a large number of variables. Xu et. al [39] studied regularized block multiconvex optimization and proposed a block coordinate descent method which can be applied to NTF problem.

In [40], Kim and Choi studied the Tucker decomposition with nonnegative constraints. Multiplicative updating algorithms for NMF are extended to solve the nonnegative Tucker decomposition. Zhou et al. [41] transformed this problem into a series of NMF problem as well, and used MU and HALS algorithms on the unfolding matrices for Tucker decomposition calculation. Some other constraints like orthogonality on

the factor matrices are also considered and studied by some researchers [42, 43]. For instance, in [43], Pan et al. proposed orthogonal nonnegative Tucker decomposition and apply the alternating direction method of multipliers (ADMM), aims to get clustering informations from the factor matrices and their joint connection weight from the core tensor. Besides these two standard and well-known decompositions, some other models are designed for the specific applications. For instance, for blind unmixing of hyperspectral problem, Qian et al. [44] proposed a model which is derived from block term decomposition (BTD) and applied alternating least square method to solve it.

1.1 The Contribution

The main aim of this paper is to propose and study Nonnegative Low Rank Tensor Approximation (NLRT) for applications of multi-dimensional images. Our approach is completely different from classical NTF which has been studied for many years. For a given nonnegative tensor, the classical NTF approach is to determine nonnegative low rank tensor by computing factor matrices or tensors (for example, CPD finds factor matrices while Tucker decomposition finds core tensor and factor matrices), such that the distance between this nonnegative low rank tensor and given tensor is as small as possible. The proposed NLRT approach is different with classical NTF. It determines a nonnegative low rank tensor without using decompositions or factorization methods. The minimized distance by the proposed NLRT method can be smaller than that by the NTF method, and it implies that the proposed NLRT method can obtain a better low rank tensor approximation. The proposed NLRT approximation algorithm is derived by using the alternating projection on the product of low rank matrix manifolds and the non-negativity property. We show the convergence of the alternating projection by constructing two projections which combine a projection of low rank matrix manifolds and the nonnegative projection, and a projection of taking average of tensors. Experimental results for synthetic data and multi-dimensional images are presented to demonstrate the above mentioned advantages of the proposed NLRT method compared the NTF methods.

The paper is organized as follows. In Section 2, we review tensor operations and decompositions, and present our algorithm. In Section 3, we show the convergence of the proposed alternating projections. In Section 4, numerical results are presented to demonstrate the proposed algorithm. Finally, some concluding remarks and future research work are given in Section 4.

2 Nonnegative Low Rank Tensor Approximation

2.1 Tensor Operations and Decompositions

An m -dimensional tensor \mathcal{A} is a multi-dimensional array, i.e., $\mathcal{A} \in \mathbb{R}^{n_1 \times n_2 \times \dots \times n_m}$. We denote its (i_1, i_2, \dots, i_m) -th entry of \mathcal{A} as $\mathcal{A}_{i_1 i_2 \dots i_m}$. The inner product of two same-sized tensors \mathcal{A} and \mathcal{B} is defined as

$$\langle \mathcal{A}, \mathcal{B} \rangle := \sum_{i_1, i_2, \dots, i_m} \mathcal{A}_{i_1 i_2 \dots i_m} \cdot \mathcal{B}_{i_1 i_2 \dots i_m}.$$

The Frobenius norm of an m -dimensional tensor \mathcal{A} is then defined as

$$\|\mathcal{A}\|_F := \sqrt{\langle \mathcal{A}, \mathcal{A} \rangle} = \left(\sum_{i_1, i_2, \dots, i_m} \mathcal{A}_{i_1 i_2 \dots i_m}^2 \right)^{\frac{1}{2}}.$$

The i -th unfolding of \mathcal{A} is defined as $\mathbf{A}_i \in \mathbb{R}^{n_i \times (n_{i+1} \dots n_m n_1 \dots n_{i-1})}$. In the following discussion, we will introduce two well-known tensor decompositions.

CP decomposition (CPD) [45–47]: Given a tensor $\mathcal{A} \in \mathbb{R}^{n_1 \times n_2 \times \dots \times n_m}$, the CANDECOMP/PARAFAC decomposition (CPD) is defined as follows:

$$\mathcal{A} = \sum_{z=1}^Z \lambda_z \mathbf{a}^{z,1} \otimes \mathbf{a}^{z,2} \otimes \dots \otimes \mathbf{a}^{z,m}. \quad (2)$$

Note that

$$\mathcal{A}_{i_1, i_2, \dots, i_m} = \sum_{z=1}^Z \lambda_z \mathbf{a}_{i_1}^{z,1} \mathbf{a}_{i_2}^{z,2} \dots \mathbf{a}_{i_m}^{z,m}, \quad (3)$$

where \otimes denotes the outer product of vectors, $\lambda^y \in \mathbb{R}^Z$, $\mathbf{a}^{z,i} \in \mathbb{R}^{n_i}$. The minimal value of Z such that CP decomposition exists is called the CP rank of \mathcal{A} .

Tucker decomposition [47–49]: Given a tensor $\mathcal{A} \in \mathbb{R}^{n_1 \times n_2 \times \dots \times n_m}$, the Tucker decomposition is defined as follows:

$$\mathcal{A} = \mathcal{G} \times_1 \mathbf{U}^{(1)} \times_2 \mathbf{U}^{(2)} \times_3 \dots \times_m \mathbf{U}^{(m)}, \quad (4)$$

i.e.,

$$\mathcal{A}_{i_1, \dots, i_m} = \sum_{j_1, \dots, j_m} \mathcal{G}_{j_1, \dots, j_m} \mathbf{U}_{i_1, j_1}^{(1)} \dots \mathbf{U}_{i_m, j_m}^{(m)}, \quad (5)$$

where $\mathcal{G} = (\mathcal{G}_{j_1, j_2, \dots, j_m}) \in \mathbb{R}^{J_1 \times J_2 \times \dots \times J_m}$, $\mathbf{U}^{(k)}$ is a n_k -by- J_k matrix where its columns are mutually orthogonal, \times_k denotes the k -mode matrix product of a tensor defined by

$$(\mathcal{G} \times_k \mathbf{U}^{(k)})_{j_1 \dots j_{k-1} i_k j_{k+1} \dots j_m} = \sum_{j_k=1}^{J_k} \mathcal{G}_{j_1 \dots j_{k-1} j_k j_{k+1} \dots j_m} \mathbf{U}_{i_k, j_k}^{(k)}.$$

The Tucker (or multilinear) rank of \mathcal{A} is defined by (J_1, J_2, \dots, J_m) .

When the nonnegativity constraints are imposed on the factor matrices generated by CPD or Tucker decompositions, the models given in (2) and (4) refer to be nonnegative tensor factorization and nonnegative Tucker decomposition respectively. Nonnegative tensor factorization [26, 36, 38, 39] and nonnegative Tucker decomposition [40–44] models and algorithms were developed to deal with nonnegative tensor applications.

2.2 The Proposed Model

In [50, 51], Song and Ng proposed a new algorithm for computing nonnegative low rank matrix approximation for nonnegative matrices. Instead of using matrix factorization in (1), their method is to determine a rank r nonnegative matrix such that the distance between such matrix and the given nonnegative matrix is as small as possible:

$$\min_{\text{rank}(\mathbf{X})=r, \mathbf{X} \geq 0} \|\mathbf{A} - \mathbf{X}\|_F^2. \quad (6)$$

They have shown the convergence of the proposed algorithm based on the projection onto a manifold of rank r matrices and the projection onto nonnegative matrices.

The main purpose of this paper is to develop nonnegative low rank tensor approximation for nonnegative tensors. The idea is to find a nonnegative low rank tensor $\mathcal{X} \in \mathbb{R}^{n_1 \times \dots \times n_m}$ such that the distance between \mathcal{X} and \mathcal{A} is as small as possible. Mathematically, it can be formulated as the following optimization problem

$$\min_{\text{rank}(\mathbf{X}_k)=r_k(k=1,\dots,m), \mathcal{X} \geq 0} \sum_{k=1}^m \|\mathbf{A}_k - \mathbf{X}_k\|_F^2, \quad (7)$$

where \mathbf{X}_k and \mathbf{A}_k are the k -th mode of unfolding matrix of \mathcal{X} and \mathcal{A} , respectively. The sizes of \mathbf{A}_k and \mathbf{X}_k are n_k -by- N_k with $N_k = \prod_{i \neq k}^n n_i$. According to the singular value decomposition of \mathbf{X}_k :

$$\mathbf{X}_k = \mathbf{P}_k \mathbf{\Sigma}_k \mathbf{Q}_k^t,$$

where \mathbf{P}_k is n_k -by- r_k with orthonormal columns, $\mathbf{\Sigma}_k$ is a diagonal matrix of size r_k -by- r_k , and \mathbf{Q}_k is N_k -by- r_k with orthonormal columns (\mathbf{Q}_k^t is the transpose of \mathbf{Q}_k), a nonnegative low rank tensor \mathcal{X} can be expressed as follows:

$$\mathcal{X} = \mathcal{S} \times_1 \mathbf{P}_1 \times_2 \mathbf{P}_2 \times_3 \dots \times_m \mathbf{P}_m.$$

Here $\mathcal{S} \in \mathbb{R}^{r_1 \times r_2 \times \dots \times r_m}$:

$$\mathcal{S} = \mathcal{X} \times_1 \mathbf{P}_1^t \times_2 \mathbf{P}_2^t \times_3 \dots \times_m \mathbf{P}_m^t$$

and thus \mathcal{X} has a multilinear rank (r_1, r_2, \dots, r_m) .

2.3 The Proposed Algorithm

We note from (7) that there are m manifolds of low rank matrices, and the constraints of nonnegativity to be considered in the optimization. In this subsection, we propose to solve (7) by using the averaged projection method which is a replacement of the alternating projections on many manifolds and the constraints of nonnegativity. Let

$$\mathbf{M}_k = \{\mathcal{W} \in \mathbb{R}^{n_1 \times \dots \times n_m} \mid \text{rank}(\mathbf{W}_k) = r_k, k = 1, \dots, m\} \quad (8)$$

denote the set of tensors which their k -mode unfolding matrices has fixed rank r_k , and

$$\mathbf{M} = \{\mathcal{W} \in \mathbb{R}^{n_1 \times \dots \times n_m} \mid \mathcal{W}_{i_1 i_2 \dots i_m} \geq 0\} \quad (9)$$

denote the set of nonnegative tensors.

Denote “fold $_k$ ” as the operator that fold a matrix into a tensor along the k -mode. Then by the Eckart-Young-Mirsky theorem [52], the projections that project an given tensor \mathcal{W} onto \mathbf{M}_k , can be expressed as follows:

$$\pi_k(\mathcal{W}) = \text{fold}_k \left(\sum_{i=1}^{r_i} \sigma_i(\mathbf{W}_k) u_i(\mathbf{W}_k) v_i(\mathbf{W}_k)^T \right), \quad k = 1, \dots, m, \quad (10)$$

where \mathbf{W}_k is the k -mode unfolding matrix of \mathcal{W} , $\sigma_i(\mathbf{W}_k)$ is the i -th singular values of \mathbf{W}_k , and their corresponding left and right singular vectors: $u_i(\mathbf{W}_k)$ and $v_i(\mathbf{W}_k)$. The

projection that projects an given tensor onto the nonnegative tensor manifold \mathcal{M} can be expressed as follows:

$$\pi(\mathcal{W}) = \begin{cases} \mathcal{W}_{i_1 i_2 \dots i_m}, & \text{if } \mathcal{W}_{i_1 i_2 \dots i_m} \geq 0, \\ 0, & \text{if } \mathcal{W}_{i_1 i_2 \dots i_m} < 0. \end{cases} \quad (11)$$

In our proposed algorithm, we consider the following two sets of tensors in the product space $\mathbb{R}^{n_1 \times \dots \times n_m} \times \dots \times \mathbb{R}^{n_1 \times \dots \times n_m}$ (m times):

$$\Omega_1 = \{\mathcal{W} = (\mathcal{W}_1, \mathcal{W}_2, \dots, \mathcal{W}_m) : \mathcal{W}_1 = \mathcal{W}_2 = \dots = \mathcal{W}_m \in \mathbf{M}\} \quad (12)$$

and

$$\Omega_2 = \mathbf{M}_1 \times \mathbf{M}_2 \dots \times \mathbf{M}_m = \{\mathcal{W} = (\mathcal{W}_1, \mathcal{W}_2, \dots, \mathcal{W}_m) : \mathcal{W}_1 \in \mathbf{M}_1, \mathcal{W}_2 \in \mathbf{M}_2, \dots, \mathcal{W}_m \in \mathbf{M}_m\}. \quad (13)$$

Note that \mathbf{M} is a convex set and an affine manifold, thus Ω_1 is also. As $\mathbf{M}_i, i = 1, \dots, m$ are C^∞ manifolds (Example 2 in [53]), Ω_2 is a product of C^∞ manifold. Now we define the two projections onto Ω_1 and Ω_2 in the alternating projections algorithm. The first projection π_{Ω_1} is given by

$$\begin{aligned} & \pi_{\Omega_1}(\mathcal{W}_1, \dots, \mathcal{W}_m) \\ &= \left(\frac{1}{m} (\pi(\mathcal{W}_1) + \dots + \pi(\mathcal{W}_m)), \dots, \frac{1}{m} (\pi(\mathcal{W}_1) + \dots + \pi(\mathcal{W}_m)) \right), \end{aligned} \quad (14)$$

where π is defined in (11). The second projection π_{Ω_2} is given by

$$\pi_{\Omega_2}(\mathcal{W}) = (\pi_1(\mathcal{W}), \dots, \pi_m(\mathcal{W})), \quad (15)$$

where π_k ($k = 1, \dots, m$) are defined in (10). The proposed algorithm is summarized in Algorithm 1. With input nonnegative tensor \mathcal{A} , the algorithm computes the projections π_{Ω_1} and π_{Ω_2} alternately until it is convergent. Note that the dominant overall computational cost of Algorithm 1 can be expressed as the SVDs of m unfolding matrices with sizes n_k by $N_k = \prod_{i \neq k} n_i$, respectively, which leads to a total of $O((\prod_{j=1}^m n_j) \sum_{i=1}^m r_i)$ flops.

Algorithm 1 Alternating Projections Algorithm

Input: Given a nonnegative tensor $\mathcal{A} \in \mathbb{R}^{n_1 \times \dots \times n_m}$, this algorithm computes a Tucker rank (r_1, r_2, \dots, r_m) nonnegative tensor close to \mathcal{A} with respect to (7).

1: Initialize $\mathcal{Z}_1^{(0)} = \dots = \mathcal{Z}_m^{(0)} = \mathcal{A}$ and $\mathcal{Z}^{(0)} = (\mathcal{Z}_1^{(0)}, \mathcal{Z}_2^{(0)}, \dots, \mathcal{Z}_m^{(0)})$

2: **for** $s = 1, 2, \dots$ (s is the iteration number)

3: $(\mathcal{Y}_1^{(s)}, \mathcal{Y}_2^{(s)}, \dots, \mathcal{Y}_m^{(s)}) = \pi_{\Omega_1}(\mathcal{Z}_1^{(s-1)}, \mathcal{Z}_2^{(s-1)}, \dots, \mathcal{Z}_m^{(s-1)});$

4: $(\mathcal{Z}_1^{(s)}, \mathcal{Z}_2^{(s)}, \dots, \mathcal{Z}_m^{(s)}) = \pi_{\Omega_2}(\mathcal{Y}_1^{(s)}, \mathcal{Y}_2^{(s)}, \dots, \mathcal{Y}_m^{(s)});$

5: **end**

Output: $\mathcal{Z}^{(s)} = (\mathcal{Z}_1^{(s)}, \mathcal{Z}_2^{(s)}, \dots, \mathcal{Z}_m^{(s)})$ when the stopping criterion is satisfied.

3 The Convergence Analysis

The framework of this algorithm is the same as the convex case for finding a point in the intersection of several closed sets, while the projection sets here are two product

manifolds. In [53], Lewis and Malick proved that a sequence of alternating projections converges locally linearly if the two projected sets are C^2 -manifolds intersecting transversally. Lewis et al. [54] proved local linear convergence when two projected sets intersecting nontangentially in the sense of linear regularity, and one of the sets is super regular. Later Bauschke et al. [55, 56] investigated the case of nontangential intersection further and proved linear convergence under weaker regularity and transversality hypotheses. In [57], Noll and Rondepierre generalized the existing results by studying the intersection condition of the two projected sets. They established local convergence of alternating projections between subanalytic sets under a mild regularity hypothesis on one of the sets. Here we analyze the convergence of the alternating projections algorithm by using the results in [57].

We remark that the sets Ω_1 and Ω_2 given in (12) and (13) respectively are two C^∞ smooth manifolds which are not closed. The convergence cannot be derived directly by applying the convergence results of alternating projections between two closed subanalytic sets. By using the results in variational analysis and differential geometry, the main convergence results are shown in the following theorem.

Theorem 1. *Let $M_i, i = 1, \dots, m$ and M be the manifolds given in (8) and (9) respectively. Let $x^* \in M_1 \cap \dots \cap M_m \cap M \neq \emptyset$. Then there exists a neighborhood U of x^* such that whenever a sequence $\mathcal{Z}^{(s)}$ derived by Algorithm 1 enters U , then it converges to some $Z^* \in M_1 \cap \dots \cap M_m \cap M$ with rate $\|\mathcal{Z}^{(s)} - Z^*\|_F = O(s^{-\delta})$ for some $\delta \in (0, +\infty)$.*

In order to show Theorem 1, it is necessary to study Hölder regularity and separable intersection. For detailed discussion, we refer to Noll and Rondepierre [57].

Definition 1. [57] *Let A and B be two sets of points in a Hilbert space equipped with the inner product $\langle \cdot, \cdot \rangle$ and the norm $\|\cdot\|$. Let $\sigma \in [0, 1)$. The set B is σ -Hölder regular with respect to A at $x^* \in A \cap B$ if there exists a neighborhood U of x^* and a constant $c > 0$ such that for every $y^+ \in A \cap U$ and every $x^+ \in p_B(y^+) \cap U$, one has*

$$\text{Ball}(y^+, (1+c)r) \cap \{x \mid y^+ = p_A(x), \langle y^+ - x^+, x - x^+ \rangle > \sqrt{c}r^{\sigma+1}\|x - x^+\|\} \cap B = \emptyset,$$

where $r = \|y^+ - x^+\|$. Note that $p_B(y^+)$ is the projection of y^+ onto B and $p_A(x)$ is the projection of x onto A , with respect to the norm. We say that B is Hölder regular with respect to A if it is σ -Hölder regular with respect to A for every $\sigma \in [0, 1)$.

Hölder regularity is mild compared with some other regularity concepts such as the prox-regularity [58], Clarke regularity [59] and super-regularity [60].

Definition 2. [57] *Let A and B be two sets of points in a Hilbert space equipped with the inner product $\langle \cdot, \cdot \rangle$ and the norm $\|\cdot\|$. We say B intersects separably A at $x^* \in A \cap B$ with exponent $\omega \in [0, 2)$ and constant $\gamma > 0$ if there exist a neighborhood U of x^* such that for every building block $z \rightarrow y^+ \rightarrow z^+$ in U , the condition*

$$\langle z - y^+, z^+ - y^+ \rangle \leq (1 - \gamma\|z^+ - y^+\|^\omega)\|y - z^+\|\|z^+ - y^+\| \quad (16)$$

holds, i.e., it is equivalent to

$$\frac{1 - \cos \alpha}{\|y^+ - z^+\|^\omega} \geq \gamma,$$

where y^+ is a projection point of z onto A , z^+ is a projection point of y onto B , and α is the angle between $z - y^+$ and $z^+ - y^+$.

This separable intersection definition is a new geometric concept which generalized the transversal intersection [53], the linear regular intersection [54], and the intrinsic transversality intersection [61]. It has been shown that the definitions of these three kinds of intersections imply $\omega = 0$ in the separable intersection.

Proof of Theorem 1. It is clear that finding a point in $M_1 \cap \dots \cap M_m \cap M$ is equivalent to finding a point in the intersection of Ω_1 and Ω_2 .

The first task is to show that Ω_2 intersects separably Ω_1 at $\mathcal{X}^* \in \Omega_1 \cap \Omega_2$ with exponent $\omega \in (0, 2)$. Define $f : \Omega_1 \rightarrow \mathbb{R}$ as

$$f(\mathcal{X}) = \delta_{\Omega_1}(\mathcal{X}) + \frac{1}{2}d_{\Omega_2}^2(\mathcal{X}), \quad \mathcal{X} = (\mathcal{X}_1, \mathcal{X}_2, \dots, \mathcal{X}_m) \in \Omega_1, \quad (17)$$

with

$$\delta_{\Omega_1}(\mathcal{X}) = \begin{cases} 0 & \text{if } \mathcal{X} \in \Omega_1, \\ +\infty & \text{otherwise} \end{cases}$$

and

$$d_{\Omega_2}(\mathcal{X}) = \min\{\|\mathcal{X} - \mathcal{W}\|_F : \mathcal{W} \in \Omega_2\}.$$

It follows the definition of $f(\mathcal{X})$ that $f(\mathcal{X}^*) = 0$ and \mathcal{X}^* is a critical point of f .

Recall that Ω_1 and Ω_2 are two C^∞ manifolds. Then f is locally Lipschitz continuous, i.e., for each $\mathcal{X} \in \Omega_1$, there is an $r > 0$ such that f is Lipschitz continuous on the open ball of center \mathcal{X} with radius r . Assume that (\mathbf{V}, ψ) is a local smooth chart of Ω_1 around \mathcal{X}^* with bounded \mathbf{V} . Therefore, $f(\mathbf{V})$ is bounded by the fact that f is local Lipschitz continuous. According to the definition of semi-algebraic function [62], we can deduce that $f \circ \psi^{-1}$ is also semi-algebraic. Then the Kurdyka-Łojasiewicz inequality [63] for $f \circ \psi^{-1}$ holds for $\bar{\mathcal{W}} := \psi(\mathcal{X}^*)$. It implies that there exist $\eta \in (0, \infty)$ and a concave function $\tau : [0, \eta]$ such that

- (i) $\tau(0) = 0$;
- (ii) τ is C^1 ;
- (iii) $\tau' > 0$ on $(0, \eta)$;
- (iv) for all $\mathcal{W} \in \psi(\mathbf{V}) = \mathbf{U}$ with $f \circ \psi^{-1}(\bar{\mathcal{W}}) < f \circ \psi^{-1}(\mathcal{W}) < f \circ \psi^{-1}(\bar{\mathcal{W}}) + \eta$, we have

$$\tau'(f \circ \psi^{-1}(\mathcal{W}) - f \circ \psi^{-1}(\bar{\mathcal{W}})) \text{dist}(0, \partial(f \circ \psi^{-1})(\mathcal{W})) \geq 1.$$

Moreover, τ is analytic on \mathbf{V} , thus $D(\psi)$ is continuous on \mathbf{V} , where D is the differential operator. For every compact subset \mathbf{K} in \mathbf{V} , there exists $C_{\mathbf{K}} := \sup_{\mathcal{W} \in \mathbf{K}} \|D(\psi(\mathcal{W}))\|$, where $\|\cdot\|$ denotes the operator norm. Suppose that \mathbf{V}' is an open set containing \mathcal{X}^* in \mathbf{V} such that $\mathbf{K} = \text{cl}(\mathbf{V}') \subset \text{int}(\mathbf{V})$ is compact ($\text{cl}(\mathbf{V}')$ denotes the closure of \mathbf{V}' and $\text{int}(\mathbf{V})$ denotes the interior of \mathbf{V}). Then, for every $\mathcal{X} \in \mathbf{V}'$ with $f(\mathcal{X}^*) < f(\mathcal{X}) < f(\mathcal{X}^*) + \eta$, we have

$$C_{\mathbf{K}}\tau'(f(\mathcal{X}) - f(\mathcal{X}^*)) \text{dist}(0, \hat{\partial}(f(\mathcal{X}))) \geq 1, \quad (18)$$

where $\hat{\partial}f(\mathcal{X})$ is the Fréchet subdifferential of f . We see that the Kurdyka-Łojasiewicz inequality is satisfied for f given in (17).

Here we construct a function $\tau = t^{1-\theta}$ which satisfies (i)-(iv). Because $f(\mathcal{X}^*) = 0$, (18) becomes

$$C_{\mathbf{K}}\tau'(f(\mathcal{X})) \text{dist}(0, \hat{\partial}(f(\mathcal{X}))) \geq 1.$$

Since $\tau'(t) = (1 - \theta)t^{-\theta}$, there always exists a neighborhood \mathbb{U} of $\mathcal{X}^* \in \Omega_1 \cap \Omega_2$ such that $C_K(1 - \theta)|f(\mathcal{X})|^{-\theta}\|g\|_F \geq 1$, i.e.,

$$|f(\mathcal{X})|^{-\theta}\|g\|_F \geq c, \quad \text{with } c = \frac{1}{C_K(1 - \theta)}, \quad (19)$$

for all $\mathcal{X} \in \Omega_1 \cap \mathbb{U}$ and every $g \in \hat{\partial}f(\mathcal{X})$.

In Algorithm 1, we construct the following sequences according to Definition 2:

$$\mathcal{Z} \rightarrow \mathcal{Y}^+ \rightarrow \mathcal{Z}^+.$$

Here \mathcal{Y}^+ is the projection $\pi_{\Omega_1}(\mathcal{Z})$ and \mathcal{Z}^+ is the projection $\pi_{\Omega_2}(\mathcal{Y}^+)$. Suppose \mathcal{Z} and \mathcal{Z}^+ are in \mathbb{U} , $\mathcal{Y}^+ \in \mathbb{U} \cap \Omega_1$, we get the proximal normal cone to Ω_1 at \mathcal{Y}^+ :

$$\mathbb{N}_{\Omega_1}^p(\mathcal{Y}^+) = \{\lambda\mathcal{V} : \lambda \geq 0, \mathcal{Y}^+ \in \pi_{\Omega_1}(\mathcal{Y}^+ + \mathcal{V})\}.$$

According to the definition of Fréchet subdifferential, $\mathcal{G} \in \hat{\partial}f(\mathcal{Y}^+)$ if and only if $\mathcal{G} = \mathcal{V} + \mathcal{Y}^+ - \mathcal{Z}^+$ for every $\mathcal{V} \in \mathbb{N}_{\Omega_1}^p(\mathcal{Y}^+)$ of the form $\mathcal{V} = \lambda(\mathcal{Z} - \mathcal{Y}^+)$.

Note that $\mathcal{Y}^+ \in \pi_{\Omega_1}(\mathcal{Z})$, from (17), we have $f(\mathcal{Y}^+) = \frac{1}{2}d_{\Omega_2}^2(\mathcal{Y}^+)$. Substitute $f(\mathcal{Y}^+)$ into (19) gives

$$2^\theta d_{\Omega_2}(\mathcal{Y}^+)^{-2\theta} \|\lambda(\mathcal{Z} - \mathcal{Y}^+) + (\mathcal{Y}^+ - \mathcal{Z}^+)\|_F \geq c > 0,$$

for every $\lambda \geq 0$. It follows that

$$d_{\Omega_2}(\mathcal{Y}^+)^{-2\theta} \min_{\lambda \geq 0} \|\lambda(\mathcal{Z} - \mathcal{Y}^+) + (\mathcal{Y}^+ - \mathcal{Z}^+)\|_F \geq 2^{-\theta}c. \quad (20)$$

Let the angle α be the angle between the iterations, which can be defined as the angle between $\mathcal{Z} - \mathcal{Y}^+$ and $\mathcal{Z}^+ - \mathcal{Y}^+$.

Let us consider two cases.

(i) When $\alpha \leq \pi/2$,

$$\min_{\lambda \geq 0} \|\lambda(\mathcal{Z} - \mathcal{Y}^+) + (\mathcal{Y}^+ - \mathcal{Z}^+)\|_F = \|\mathcal{Y}^+ - \mathcal{Z}^+\|_F \sin \alpha,$$

Substitute it into (20), then

$$\frac{\sin \alpha}{d_{\Omega_2}(\mathcal{Y}^+)^{2\theta-1}} \geq 2^{-\theta}c.$$

Note that $1 - \cos \alpha \geq \frac{1}{2} \sin^2 \alpha$, we have

$$\frac{1 - \cos \alpha}{d_{\Omega_2}(\mathcal{Y}^+)^{4\theta-2}} \geq 2^{-2\theta-1}c^2. \quad (21)$$

when the numerator tends to 0, the denominator has to go to zero, which implies that $4\theta - 2 > 0$, i.e., $\theta > \frac{1}{2}$. Therefore, we get Ω_2 intersects Ω_1 separably with exponent $\omega = 4\theta - 2 \in (0, 2)$, the corresponding constant can be set to be $c' = 2^{-2\theta-1}c^2$.

(ii) When $\alpha > \pi/2$, which means $\cos \alpha < 0$, i.e., $1 - \cos \alpha \geq 1$. The infimum in (20) is attained at $\lambda = 0$. (20) becomes $d_{\Omega_2}(\mathcal{Y}^+)^{1-2\theta} \geq 2^{-\theta}c$. Therefore,

$$d_{\Omega_2}(\mathcal{Y}^+)^{2-4\theta} \geq 2^{-2\theta}c^2 > 2^{-2\theta-1}c^2.$$

(21) is also satisfied. According to Definition 2, Ω_2 intersects Ω_1 separably.

On the other hand, Ω_1 intersects Ω_2 separably can be proved by using the similar argument.

It follows from Theorem 1 and Corollary 4 in [57] that there exists a neighborhood V of \mathcal{X}^* such that every sequence of alternating projections that enters V converges to $\mathcal{X}^* \in \Omega_1 \cap \Omega_2$. The convergence rate is $\|\mathcal{Z}^{(s)} - \mathcal{X}^*\|_F = O(s^{-\frac{2-\omega}{2\omega}})$ and $\|\mathcal{Y}^{(s)} - \mathcal{X}^*\|_F = O(s^{-\frac{2-\omega}{2\omega}})$ with $\omega \in (0, 2)$. The result follows.

In the next section, we test our method and nonnegative tensor decomposition methods on the synthetic data and real-world data, and show the performance of the proposed alternating projections method is better than the other methods.

4 Experimental Results

The state-of-the-art methods for nonnegative tensor decompositions in Section 2.1 are used as follows.

- Nonnegative CP decomposition (NCPD). For the CP scheme approximation, we will use the hierarchical ALS algorithm (referred to as “NCPD-HALS”) proposed in [26, 36], a fixed point (FP) algorithm (referred to as “NCPD-FP”) in [35], and a block coordinate descent (BCD) method (referred to as “NCPD-BCD”) from [39].
- Nonnegative Tucker decomposition (NTD). For the Tucker scheme approximation, we apply the HALS algorithm (referred to as “NTD-HALS”), the accelerated proximal gradient algorithm (referred to as “NTD-APG”), and the plain multiple updating algorithm (referred to as “NTD-MU”) in [41] and the block coordinate descent (BCD) method (referred to as “NTD-BCD”) from [39].

In the following, we list the computational cost of these methods. The cost of the proposed NLRT method per iteration is about the same as that of NTD-type methods. As they involve the calculation of nonnegative vectors only, the cost of NCP-type methods per iteration is smaller than that of the proposed NLRT method.

Table 1: The computational cost.

| Method | Complexity | Details of most expensive computations |
|-----------|--|---|
| NCPD-BCD | $O(mr\Pi_{j=1}^m n_j)$ | Khatri-Rao product and unfolding matrices times Khatri-Rao product. |
| NCPD-HALS | $O(mr\Pi_{j=1}^m n_j)$ | Khatri-Rao product and unfolding matrices times Khatri-Rao product. |
| NCPD-FP | $O(mr\Pi_{j=1}^m n_j)$ | Khatri-Rao product and unfolding matrices times Khatri-Rao product. |
| NTD-BCD | $O(\sum_{i=1}^m \Pi_{j \neq i}^m n_j r_i (r_i + n_i))$ | The tensor-matrix multiplication and the matrix multiplication between the i -th unfolding matrix of $\mathcal{G} \times_{j=1, j \neq i} \mathbf{U}^{(j)}$ and its transpose. |
| NTD-APG | $O(\sum_{i=1}^m \Pi_{j \neq i}^m n_j r_i^2)$ | The tensor-matrix multiplications among a) the i -th factor matrix b) the transpose of the i -th unfolding matrix of $\mathcal{G} \times_{j=1, j \neq i} \mathbf{U}^{(j)}$ and c) the i -th unfolding matrix of $\mathcal{G} \times_{j=1, j \neq i} \mathbf{U}^{(j)}$. |
| NTD-HALS | $O(\sum_{i=1}^m \Pi_{j \neq i}^m n_j r_i)$ | HALS on unfolding matrices $\{\mathbf{A}_i\}_{k=1}^m$. |
| NTD-MU | $O(\sum_{i=1}^m \Pi_{j \neq i}^m n_j r_i^2)$ | MU on unfolding matrices $\{\mathbf{A}_i\}_{k=1}^m$. |
| NLRT | $O((\Pi_{j=1}^m n_j) \sum_{i=1}^m r_i)$ | SVDs of unfolding matrices $\{\mathbf{A}_i\}_{k=1}^m$. |

The stopping criterion of the proposed method and other comparison methods is that the relative difference between successive iterates is smaller than 10^{-5} . All the experiments are conducted on Intel(R) Core(TM) i9-9900K CPU@3.60GHz with 32GB of RAM using Matlab.

4.1 Synthetic Datasets

We first test different methods on synthetic datasets. We generate two kinds of synthetic data as follows:

- Test 1 (Low-rank nonnegative tensor): We generate low rank nonnegative tensors by two steps. First, a core tensor of the size $r_1 \times r_2 \times \dots \times r_m$ (i.e., multilinear rank is (r_1, r_2, \dots, r_m)) and m factor matrices of sizes $n_i \times r_i$ are generated with entries uniformly distributed in $[0, 1]$. Second, these factor matrices are multiplied to the core tensor via the tensor-matrix product and the low rank nonnegative tensors of size $n_1 \times n_2 \times \dots \times n_m$ are normalized to $[0, 1]$. Finally, we add the truncated Gaussian noise (i.e., set the negative noisy value to be 0) to the generated tensor with different signal-to-noise ratios (SNR). Given the multilinear rank (r_1, r_2, \dots, r_m) , the CP rank is cannot be larger than $\prod_{k=1}^m r_k$. Therefore, we set the CP rank in the NCPD methods from three possible values: $\{\prod_{k=1}^m r_k, \sum_{k=1}^m r_k, \max_i r_i\}$. In the results, we report the best relative approximation error in the NCPD methods.
- Test 2 (Nonnegative tensor) We randomly generate nonnegative tensors of size $n_1 \times n_2 \times \dots \times n_k \times \dots \times n_m$ where their entries follow a uniform distribution in between 0 and 1. The low rank minimizer is unknown in this setting. In the CP decomposition methods, the CP rank is set to be r . In the Tucker decomposition methods, the multilinear rank is set to be $[r, r, \dots, r]$.

We report the relative approximation error, which is defined as

$$\frac{\|\mathcal{X}_{\text{estimated}} - \mathcal{X}_{\text{groundtruth}}\|_F}{\|\mathcal{X}_{\text{groundtruth}}\|_F},$$

to measure the approximation quality. The ground truth tensor is the generated tensor without noise. The relative approximation errors of the results by different methods in Test 1 are reported in Table 2. The reported entries of all the comparison methods in the table are the average results over ten different initial guesses in CP decomposition vectors and Tucker decomposition matrices. However, the results of the proposed NLRT method are deterministic when the given nonnegative tensor is fixed. We see from Table 2 that the proposed NLRT method achieves the best performance and it is also quite robust to SNRs. On the other hand, the relative approximation errors in Test 2 are plotted in Fig. 1 with respect to different values of rank r . Again the reported entries are the average results over ten different initial guesses in the comparison methods. From Fig. 1, we can see that the proposed NLRT method and NTD-BCD perform better than the other methods. For the tensors of the size $40 \times 40 \times 40$, the superior of our method over NTD-BCD is obvious when the rank is in between 27 and 39.

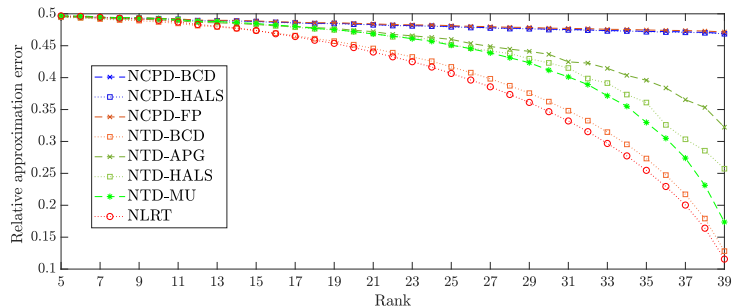
4.2 Video Data

In this subsection, we select 4 videos¹ to test our method on the task of approximation. Three videos (respectively named “foreman”, “coastguard”, and “news”) are of the size

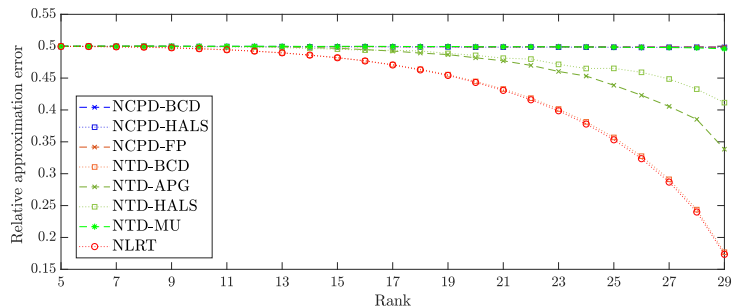
¹Videos are available at <http://trace.eas.asu.edu/yuv/> and <https://sites.google.com/site/jamiezeminzhang/publications>.

Table 2: The relative approximation errors of the results by different methods in Test 1. The **best** values are highlighted in bold.

| Tensor size: $40 \times 40 \times 40$ | | | | | Multilinear rank: $[5, 5, 5]$ | | | | |
|---|-----------|-----------|-----------|-----------|----------------------------------|-----------|-----------|-----------|------------------|
| SNR (dB) | Noisy | NCPD-BCD | NCPD-HALS | NCPD-FP | NTD-BCD | NTD-APG | NTD-HALS | NTD-MU | NLRT |
| 30 | 3.162e-02 | 1.860e-02 | 1.876e-02 | 2.007e-02 | 1.818e-02 | 2.167e-02 | 1.996e-02 | 2.546e-02 | 1.796e-02 |
| 40 | 1.000e-02 | 6.066e-03 | 7.358e-03 | 1.070e-02 | 6.411e-03 | 1.303e-02 | 1.150e-02 | 1.974e-02 | 5.663e-03 |
| 50 | 3.162e-03 | 2.122e-03 | 5.039e-03 | 8.861e-03 | 3.245e-03 | 1.227e-02 | 9.539e-03 | 1.895e-02 | 1.793e-03 |
| Tensor size: $30 \times 30 \times 30 \times 30$ | | | | | Multilinear rank: $[2, 3, 4, 5]$ | | | | |
| SNR (dB) | Noisy | NCPD-BCD | NCPD-HALS | NCPD-FP | NTD-BCD | NTD-APG | NTD-HALS | NTD-MU | NLRT |
| 30 | 3.162e-02 | 1.813e-02 | 1.845e-02 | 2.055e-02 | 1.766e-02 | 2.278e-02 | 2.023e-02 | 3.086e-02 | 1.747e-02 |
| 40 | 1.000e-02 | 6.308e-03 | 7.441e-03 | 1.203e-02 | 6.816e-03 | 1.437e-02 | 1.141e-02 | 2.721e-02 | 5.519e-03 |
| 50 | 3.162e-03 | 2.817e-03 | 4.888e-03 | 1.029e-02 | 2.454e-03 | 1.311e-02 | 1.173e-02 | 2.576e-02 | 1.750e-03 |



(a) $40 \times 40 \times 40$



(b) $30 \times 30 \times 30 \times 30$

Figure 1: Relative approximation errors on the randomly generated tensors in Test 2 with respect to the different rank settings.

$144 \times 176 \times 100$ (height \times width \times frame) and one (named “basketball”) is of the size $44 \times 256 \times 40$. Firstly, we set the multilinear rank to be (r, r, \dots, r) and the CP rank to be r . We test our method to approximate these four videos with varying r from 5 to 100. Moreover, we add the Gaussian noise to the video “coastguard” with different noise levels (SNR = 20, 30, 40, 50), and test the approximation ability for the noisy data. We plot the relative approximation errors with respect to r on four videos in Fig. 2. It can be seen that the approximation errors of the results by our method are the lowest. Fig. 3 shows the relative approximation errors on the noisy video “coastguard” with respect to the r . Similarly, our method achieves the lowest approximation errors.

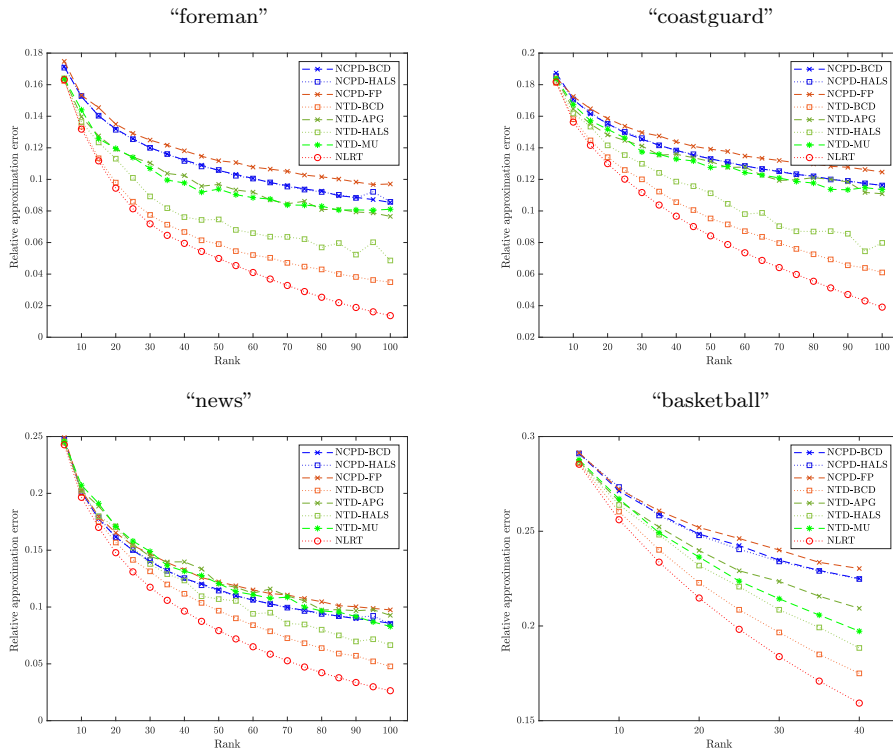


Figure 2: Relative approximation errors on the videos with respect to the different rank settings.

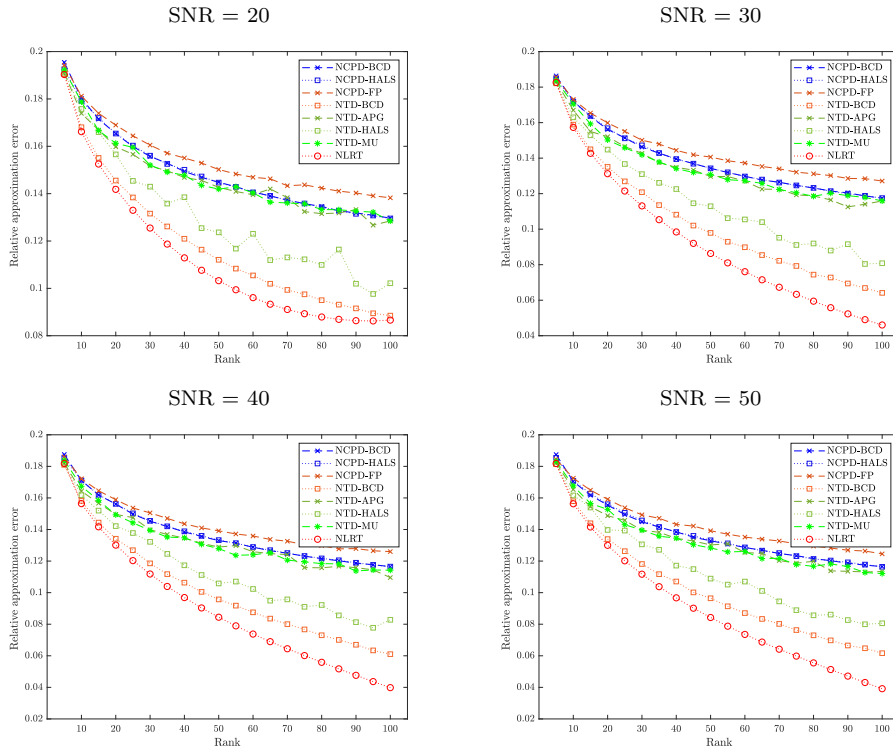


Figure 3: Relative approximation errors on the noisy video "coastguard" with respect to the different rank settings.

4.3 Hyperspectral Data

In this subsection, we test different methods on the hyperspectral data. We consider four hyperspectral images (HSIs): a subimage of Pavia City Center dataset² of the size $200 \times 200 \times 80$ (height \times width \times band), a subimage of Washington DC Mall dataset³ of size $256 \times 256 \times 160$, the RemoteImage⁴ of the size $200 \times 200 \times 89$, and a subimage of Curprite dataset⁵ of the size $150 \times 150 \times 150$.

Figs. 4 and 5 report the relative approximation errors with respect to different values of rank r . It is evidently that the relative approximation errors by our NLRT are the lowest among all the methods. It is interesting to note that the difference between our method and NTD-BCD (the second best comparison method) is more significant than that on the synthetic data. In Fig. 6, we display the pseudo-color images of the results on the Washington DC Mall dataset with multilinear rank (100,100,100) and CP-rank = 100. The pseudo-color image is composed of the 145th, 127-th, and 92-th bands as the red, green, and blue channel, respectively. In Fig. 6, we also report two image quality assessments: the mean value of the peak signal to noise ratio (MPSNR)⁶ and the mean value of the structural similarity index of all the spectral bands (MSSIM) [64]. It can be found in Fig. 6 that both visual and quality assessments of the proposed NLRT method are better than those by the other comparison methods.

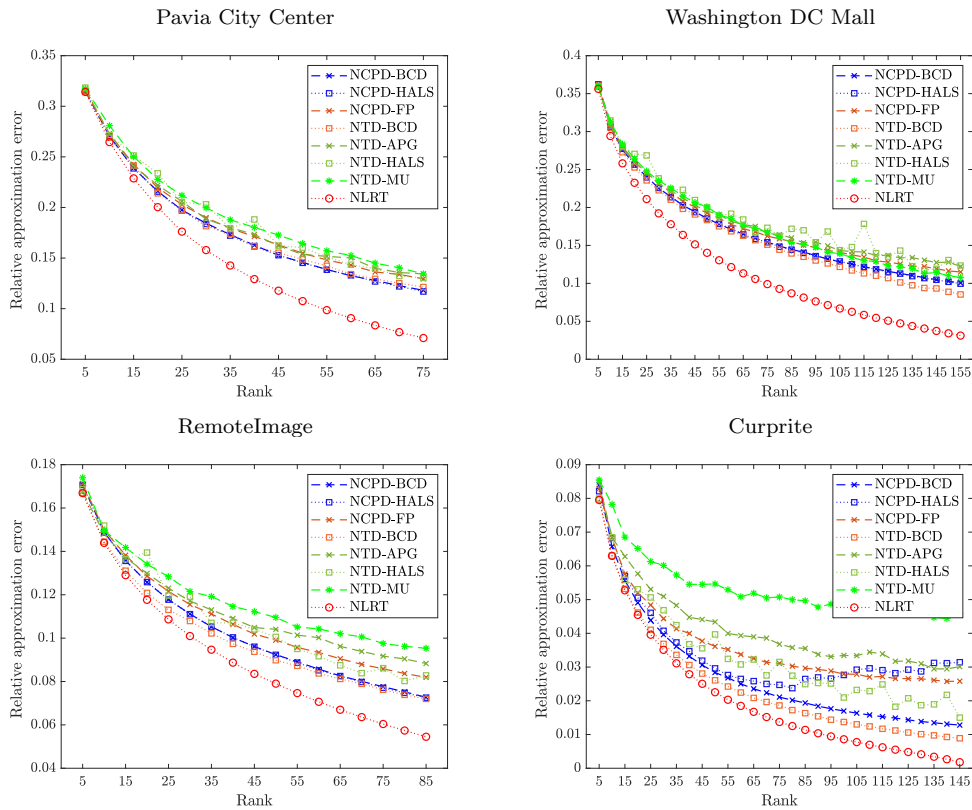


Figure 4: Relative approximation errors on 4 HSIs with respect to the different rank settings.

²Data available at http://www.ehu.es/ccwintco/index.php?title=Hyperspectral_Remote_Sensing_Scenes.

³Data available at <https://engineering.purdue.edu/biehl/MultiSpec/hyperspectral.html>.

⁴Data available at <https://www.cs.rochester.edu/~jliu/code/TensorCompletion.zip>.

⁵Data available at https://aviris.jpl.nasa.gov/data/free_data.html.

⁶https://en.wikipedia.org/wiki/Peak_signal-to-noise_ratio

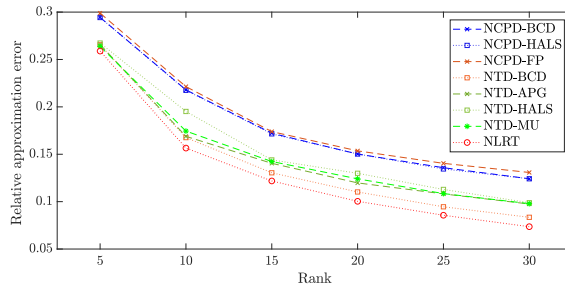


Figure 5: Relative approximation errors on the HSV with respect to the different rank settings.

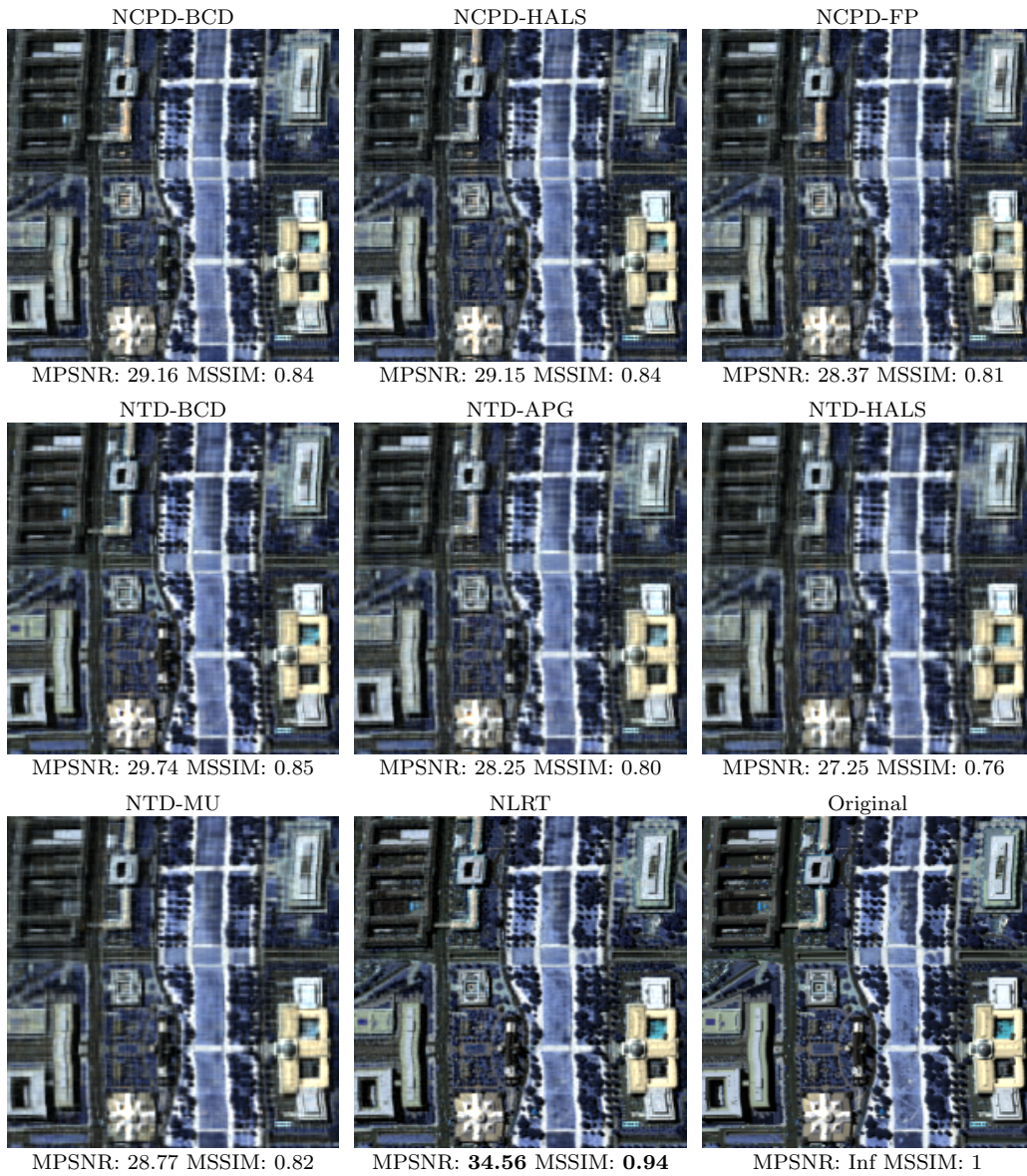


Figure 6: The pseudo-color images composed of the 145th, 127-th, and 92-th bands of the non-negative low-rank approximations by different methods when setting the rank 100 on the Washington DC Mall.

4.4 Selection of Features

One advantage of the proposed NLRT method is that it can provide a significant index based on singular values of unfolding matrices [50] that can be used to identify important singular basis vectors in the approximation. Here we take the HSI Washington DC Mall as an example. We compute the low-rank approximations of the proposed NLRT method and the other comparison methods with multilinear rank (r, r, r) and CP rank r for $r = 20, 40, 60, 80, 160$. For the approximation results by NCPD methods, we normalize the base vectors in 2 such that the ℓ_2 norms of $\mathbf{a}^{k,1}$, $\mathbf{a}^{k,2}$ and $\mathbf{a}^{k,3}$ are equal to 1, and rearrange the resulting values λ'_z in the descending order in the CP decomposition. In Fig. 7, we plot $\|\mathcal{A} - \mathcal{X}_{\text{NCPD}}(j)\|_F / \|\mathcal{A}\|_F$ with respect to j , where $\mathcal{X}_{\text{NCPD}}(j) = \sum_{k=1}^j \lambda'_k \mathbf{a}^{k,1} \otimes \mathbf{a}^{k,2} \otimes \mathbf{a}^{k,3}$. Similarly, for the results of NTD methods, we also plot $\|\mathcal{A} - \mathcal{X}_{\text{NTD}}(j)\|_F / \|\mathcal{A}\|_F$ with respect to j , where $\mathcal{X}_{\text{NTD}}(j) = [\mathcal{G} \times_1 \mathbf{U}^{(1)} \times_2 \mathbf{U}^{(2)}]_{:,:\mathbf{k}_j} \times_3 \mathbf{U}_{:,:\mathbf{k}_j}^{(3)}$, and \mathbf{k}_j indicates a vector composed of the indexes corresponding to the j largest ℓ_2 norms of $\mathbf{U}^{(3)}$'s columns. For the results by our methods, we plot $\|\mathcal{A} - \mathcal{X}_{\text{NLRT}}(j)\|_F / \|\mathcal{A}\|_F$ with respect to j , where $\mathcal{X}_{\text{NLRT}}(j) = \text{fold} \left(\sum_{i=1}^j \sigma_i(\mathbf{X}_3) \mathbf{u}_i(\mathbf{X}_3) \mathbf{v}_i^T(\mathbf{X}_3) \right)$, $\sigma_i(\mathbf{X}_3)$ is the i -th singular values of \mathbf{X}_3 , and \mathbf{X}_3 is the third-mode unfolding matrix of \mathcal{X} . The third-mode of \mathcal{X} is chosen in NTD and our NLRT, we are interested to observe how many indices required in the spectral model of given hyperspectral data.

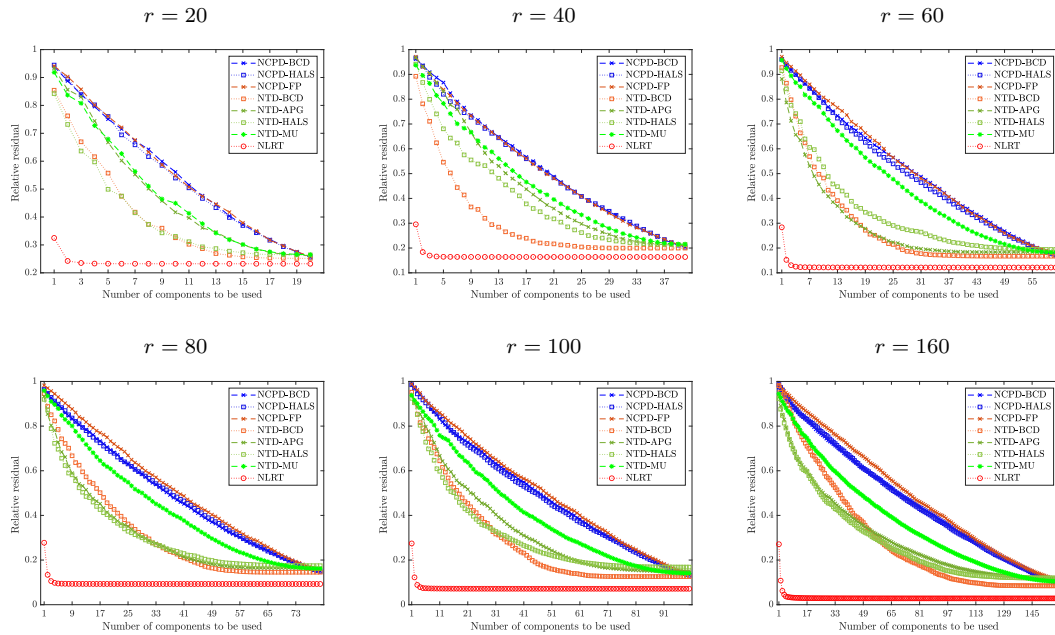


Figure 7: The comparison of relative residuals with respect to the number of mode-3 components to be used in the tensor approximation with $R = 20, 40, 60, 80, 160$ for the hyperspectral image Washington DC Mall.

In Fig. 7, we can see that when the number of components (namely j) increases, the relative residual decreases. Our NLRT could provide a significant index based on singular values to identify important singular basis vectors for the approximation. Thus, the relative residuals by the proposed NLRT algorithm are significantly smaller than those by the testing NTD and NCPD algorithms. Similar phenomena can be found in Fig. 8, in which $\mathcal{X}_{\text{NTD}}(j)$ and $\mathcal{X}_{\text{NLRT}}(j)$ are computed using the number of indices in the first or second modes of \mathcal{X} .

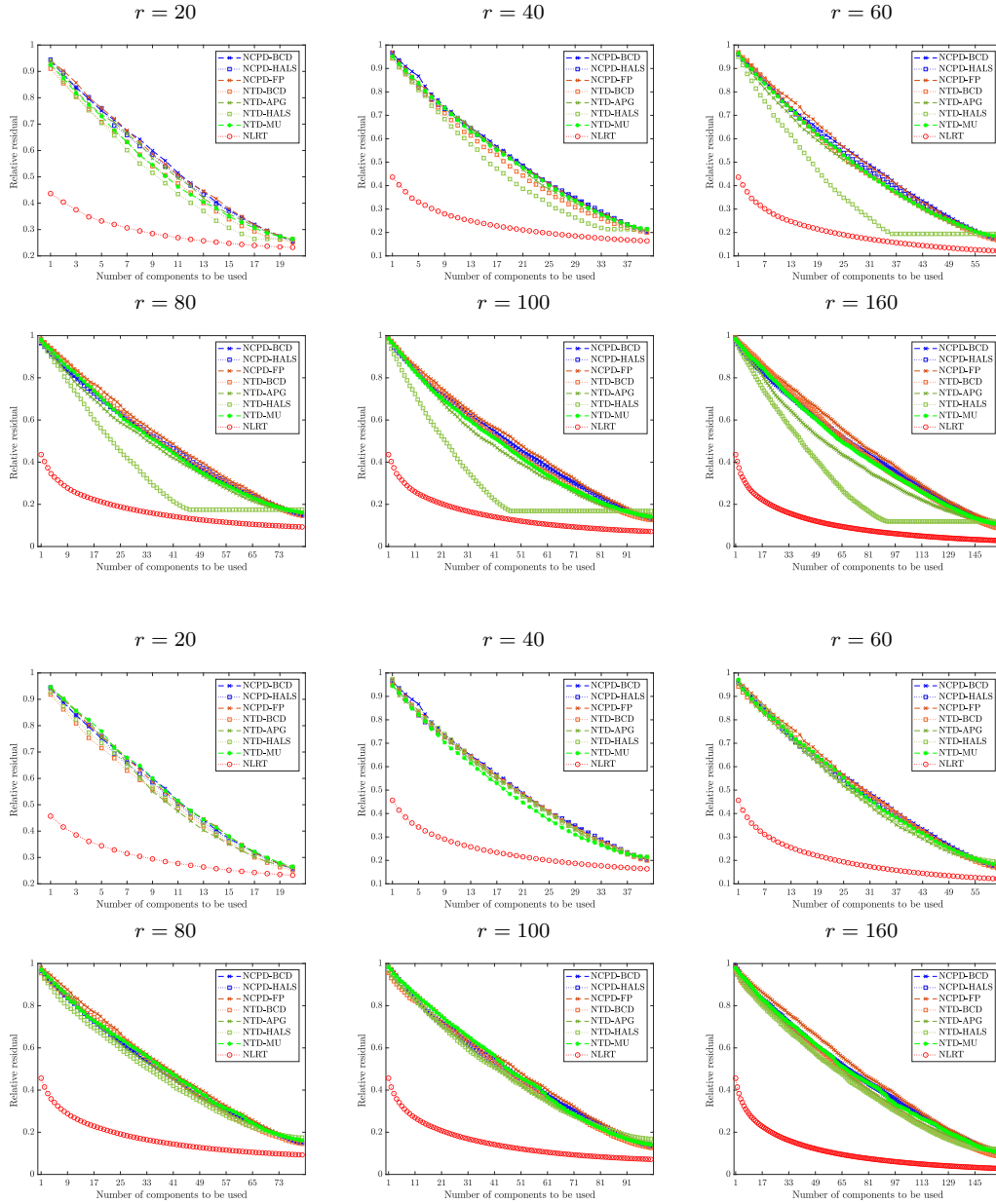


Figure 8: The comparison of relative residuals with respect to the number of the first mode (upper two rows) and the second mode (bottom two rows) components to be used in the tensor approximation with $r = 20, 40, 60, 80, 160$ for the hyperspectral image Washington DC Mall.

4.5 Image Classification

The advantage of the proposed NLRT method is that the important singular basis vectors can be identified. Such basis vectors can provide useful information for image recognition such as classification. Here we conduct hyperspectral image classification experiments on the Indian Pines dataset⁷. This data set was captured by the Airborne Visible/Infrared Imaging Spectrometer (AVIRIS) sensor over the Indian Pines test site

⁷Data available at <https://engineering.purdue.edu/~biehl/MultiSpec/hyperspectral.html>.

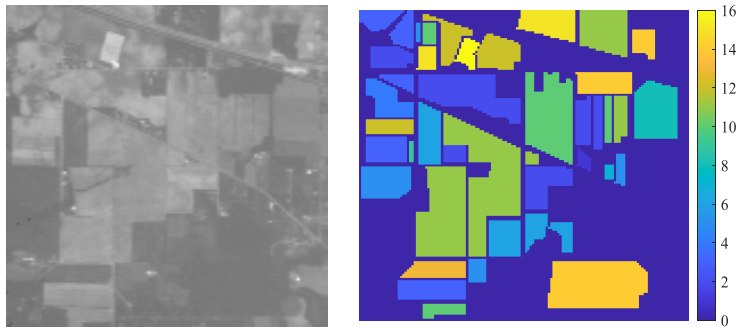


Figure 9: Indian Pines image and related ground truth categorization information. Left: the 10-th band of the original HSI. Right: the ground truth categorization map.

Table 3: The number of label samples in each class.

| No. | 1 | 2 | 3 | 4 | 5 | 6 | 7 | 8 |
|---------|---------|-----------------|------------------|---------------|---------------|-------------|------------------------------|--------------------|
| Name | Alfalfa | Corn-no till | Corn-min till | Corn | Grass-pasture | Grass-trees | Grass-pasture-mowed | Hay-windrowed |
| Samples | 46 | 1428 | 830 | 237 | 483 | 730 | 28 | 478 |
| No. | 9 | 10 | 11 | 12 | 13 | 14 | 15 | 16 |
| Name | Oat | Soybean-no till | Soybean-min till | Soybean-clean | Wheat | Woods | Buildings-Grass-Trees-Drives | Stone-Steel-Towers |
| Samples | 20 | 972 | 2455 | 593 | 205 | 1265 | 386 | 93 |

in North-western Indiana in June 1992. After removing 20 bands, which cover the region of water absorption, this HSI is of the size $145 \times 145 \times 200$. The ground truth contains 16 land cover classes as shown in Fig. 9. Therefore, we set the multilinear rank to be $(16, 16, 16)$ and the CP rank to be 16 for all the testing methods. We randomly choose s of the available labelled samples, which are exhibited in Table 3. Labelled samples from each class are used for training and the remaining samples are used for testing.

After obtaining low rank approximations, 16 singular vectors corresponding to the largest 16 singular values of the unfolding matrix of the tensor approximation along the spectral mode (the third mode) are employed for classification. We apply the k -nearest neighbour (k -NN, $k=1, 3, 5$) classifiers to identify the testing samples in the projected trained samples representation. The classification accuracy, which is defined as the portion of correctly identified entries, with respect to different s is reported in Table 4. The results in Table 4 show that the classification based on our nonnegative low rank approximation is better than the other comparison methods.

5 Conclusion

In the paper, we proposed a new idea for computing nonnegative low rank tensor approximation. We do not consider to approximate data by using classic factorization or decomposition methods. Instead, our proposed method NLRT determine a nonnegative low rank approximation to given data by taking use of low rank matrix manifolds and non-negativity property. The convergence analysis is given. Experiments in synthetic data sets and multi-dimensional image data sets are conducted to present the performance of the proposed NLRT method. It shows that NLRT is better than classical nonnegative tensor factorization methods.

Table 4: The accuracy (in terms of percentage) of the classification results on the approximations by different methods. The **best** values are highlighted in bold.

| s | Classifier | NCPD-BCD | NCPD-HALS | NCPD-FP | NTD-BCD | NTD-APG | NTD-HALS | NTD-MU | NLRT |
|-----|------------|----------|-----------|---------|---------|---------|----------|--------|--------------|
| 10 | 1-NN | 69.07 | 66.49 | 71.52 | 74.66 | 69.08 | 70.56 | 62.66 | 74.90 |
| | 3-NN | 64.31 | 61.46 | 66.77 | 69.22 | 64.73 | 65.62 | 58.94 | 70.11 |
| | 5-NN | 62.12 | 59.65 | 65.75 | 67.18 | 63.69 | 64.60 | 58.30 | 68.39 |
| 20 | 1-NN | 76.91 | 73.96 | 79.01 | 81.95 | 75.90 | 78.33 | 69.90 | 82.05 |
| | 3-NN | 72.27 | 69.58 | 74.13 | 76.51 | 72.37 | 74.07 | 65.76 | 77.49 |
| | 5-NN | 70.26 | 67.64 | 72.35 | 73.72 | 70.27 | 71.92 | 64.12 | 75.60 |
| 30 | 1-NN | 80.92 | 78.18 | 81.93 | 85.52 | 79.77 | 81.77 | 74.59 | 85.71 |
| | 3-NN | 76.37 | 73.93 | 77.79 | 80.69 | 75.90 | 78.00 | 69.69 | 81.61 |
| | 5-NN | 74.39 | 71.86 | 75.90 | 77.97 | 73.93 | 76.04 | 68.23 | 79.17 |
| 40 | 1-NN | 83.86 | 81.54 | 84.54 | 88.17 | 82.04 | 84.56 | 77.28 | 88.53 |
| | 3-NN | 79.70 | 77.49 | 80.98 | 84.11 | 78.94 | 80.81 | 73.05 | 84.87 |
| | 5-NN | 77.17 | 75.17 | 79.42 | 81.23 | 76.86 | 79.08 | 70.78 | 82.98 |
| 50 | 1-NN | 85.51 | 83.81 | 86.02 | 89.88 | 84.48 | 86.27 | 80.66 | 90.15 |
| | 3-NN | 81.55 | 79.82 | 82.90 | 86.35 | 81.40 | 82.80 | 75.59 | 86.52 |
| | 5-NN | 79.37 | 77.67 | 81.34 | 84.15 | 79.39 | 80.97 | 73.03 | 84.81 |

References

- [1] Daniel D. Lee and H. Sebastian Seung. Learning the parts of objects by non-negative matrix factorization. *Nature*, 401(6755):788–791, 1999.
- [2] David Guillaumet and Jordi Vitria. Non-negative matrix factorization for face recognition. In *Catalonian Conference on Artificial Intelligence*, pages 336–344. Springer, 2002.
- [3] David Guillaumet, Jordi Vitria, and Bernt Schiele. Introducing a weighted non-negative matrix factorization for image classification. *Pattern Recognition Letters*, 24(14):2447–2454, 2003.
- [4] Ke Chen. *Matrix preconditioning techniques and applications*, volume 19. Cambridge University Press, 2005.
- [5] Yuan Wang, Yunde Jia, Changbo Hu, and Matthew Turk. Non-negative matrix factorization framework for face recognition. *International Journal of Pattern Recognition and Artificial Intelligence*, 19(04):495–511, 2005.
- [6] Daoqiang Zhang, Songcan Chen, and Zhi-Hua Zhou. Two-dimensional non-negative matrix factorization for face representation and recognition. In *International Workshop on Analysis and Modeling of Faces and Gestures*, pages 350–363. Springer, 2005.
- [7] Chris Ding, Xiaofeng He, and Horst D Simon. On the equivalence of nonnegative matrix factorization and spectral clustering. In *Proceedings of the 2005 SIAM International Conference on Data Mining*, pages 606–610. SIAM, 2005.
- [8] Chris Ding, Tao Li, Wei Peng, and Haesun Park. Orthogonal nonnegative matrix t-factorizations for clustering. In *Proceedings of the 12th ACM SIGKDD International Conference on Knowledge Discovery and Data Mining*, pages 126–135, 2006.
- [9] Liping Jing, Jian Yu, Tiejong Zeng, and Yan Zhu. Semi-supervised clustering via constrained symmetric non-negative matrix factorization. In *International Conference on Brain Informatics*, pages 309–319. Springer, 2012.

- [10] Jianjun Liu, Zebin Wu, Zhihui Wei, Liang Xiao, and Le Sun. A novel sparsity constrained nonnegative matrix factorization for hyperspectral unmixing. In *2012 IEEE International Geoscience and Remote Sensing Symposium*, pages 1389–1392. IEEE, 2012.
- [11] Meng Chen, Wen-Sheng Chen, Bo Chen, and Binbin Pan. Non-negative sparse representation based on block nmf for face recognition. In *Chinese Conference on Biometric Recognition*, pages 26–33. Springer, 2013.
- [12] Ya Liu, Xian-Zhang Pan, Rong-Jie Shi, Yan-Li Li, Chang-Kun Wang, and Zhi-Ting Li. Predicting soil salt content over partially vegetated surfaces using non-negative matrix factorization. *IEEE Journal of Selected Topics in Applied Earth Observations and Remote Sensing*, 8(11):5305–5316, 2015.
- [13] Michael W Berry and Jacob Kogan. *Text mining: applications and theory*. John Wiley & Sons, 2010.
- [14] Tao Li and Chris Ding. The relationships among various nonnegative matrix factorization methods for clustering. In *Sixth International Conference on Data Mining (ICDM'06)*, pages 362–371. IEEE, 2006.
- [15] V. Paul Pauca, Fariar Shahnaz, Michael W. Berry, and Robert J. Plemmons. Text mining using non-negative matrix factorizations. In *Proceedings of the 2004 SIAM International Conference on Data Mining*, pages 452–456. SIAM, 2004.
- [16] Wei Xu, Xin Liu, and Yihong Gong. Document clustering based on non-negative matrix factorization. In *Proceedings of the 26th Annual International ACM SIGIR Conference on Research and Development in Informaion Retrieval*, pages 267–273, 2003.
- [17] Philip M Kim and Bruce Tidor. Subsystem identification through dimensionality reduction of large-scale gene expression data. *Genome Research*, 13(7):1706–1718, 2003.
- [18] Hyunsoo Kim and Haesun Park. Sparse non-negative matrix factorizations via alternating non-negativity-constrained least squares for microarray data analysis. *Bioinformatics*, 23(12):1495–1502, 2007.
- [19] Alberto Pascual-Montano, Jose Maria Carazo, Kieko Kochi, Dietrich Lehmann, and Roberto D Pascual-Marqui. Nonsmooth nonnegative matrix factorization (nsNMF). *IEEE Transactions on Pattern Analysis and Machine Intelligence*, 28(3):403–415, 2006.
- [20] Guoli Wang, Andrew V. Kossenkov, and Michael F. Ochs. LS-NMF: a modified non-negative matrix factorization algorithm utilizing uncertainty estimates. *BMC Bioinformatics*, 7(1):175, 2006.
- [21] Andrzej Cichocki, Rafal Zdunek, Anh Huy Phan, and Shun-ichi Amari. *Nonnegative matrix and tensor factorizations: applications to exploratory multi-way data analysis and blind source separation*. John Wiley & Sons, 2009.
- [22] Pentti Paatero and Unto Tapper. Positive matrix factorization: A non-negative factor model with optimal utilization of error estimates of data values. *Environmetrics*, 5(2):111–126, 1994.

- [23] Daniel D. Lee and H. Sebastian Seung. Algorithms for non-negative matrix factorization. In *Advances in Neural Information Processing Systems*, pages 556–562, 2001.
- [24] Zhijian Yuan and Erkki Oja. Projective nonnegative matrix factorization for image compression and feature extraction. In *Scandinavian Conference on Image Analysis*, pages 333–342. Springer, 2005.
- [25] Nicolas Gillis and François Glineur. Accelerated multiplicative updates and hierarchical ALS algorithms for nonnegative matrix factorization. *Neural Computation*, 24(4):1085–1105, 2012.
- [26] Andrzej Cichocki, Rafal Zdunek, and Shun-ichi Amari. Hierarchical ALS algorithms for nonnegative matrix and 3D tensor factorization. In *International Conference on Independent Component Analysis and Signal Separation*, pages 169–176. Springer, 2007.
- [27] Chih-Jen Lin. Projected gradient methods for nonnegative matrix factorization. *Neural Computation*, 19(10):2756–2779, 2007.
- [28] Da Kuang, Chris Ding, and Haesun Park. Symmetric nonnegative matrix factorization for graph clustering. In *Proceedings of the 2012 SIAM International Conference on Data Mining*, pages 106–117. SIAM, 2012.
- [29] Da Kuang, Sangwoon Yun, and Haesun Park. Symnmf: nonnegative low-rank approximation of a similarity matrix for graph clustering. *Journal of Global Optimization*, 62(3):545–574, 2015.
- [30] Nicolas Gillis and Stephen A Vavasis. Fast and robust recursive algorithms for separable nonnegative matrix factorization. *IEEE Transactions on Pattern Analysis and Machine Intelligence*, 36(4):698–714, 2013.
- [31] Junjun Pan and Nicolas Gillis. Generalized separable nonnegative matrix factorization. *IEEE Transactions on Pattern Analysis and Machine Intelligence*, 2019.
- [32] Seungjin Choi. Algorithms for orthogonal nonnegative matrix factorization. In *2008 IEEE International Joint Conference on Neural Networks (IEEE World Congress on Computational Intelligence)*, pages 1828–1832. IEEE, 2008.
- [33] Ganesh R Naik. *Non-negative matrix factorization techniques*. Springer, 2016.
- [34] Nicholas D Sidiropoulos, Lieven De Lathauwer, Xiao Fu, Kejun Huang, Evangelos E Papalexakis, and Christos Faloutsos. Tensor decomposition for signal processing and machine learning. *IEEE Transactions on Signal Processing*, 65(13):3551–3582, 2017.
- [35] Max Welling and Markus Weber. Positive tensor factorization. *Pattern Recognition Letters*, 22(12):1255–1261, 2001.
- [36] Andrzej Cichocki and Anh-Huy Phan. Fast local algorithms for large scale non-negative matrix and tensor factorizations. *IEICE Transactions on Fundamentals of Electronics, Communications and Computer Sciences*, 92(3):708–721, 2009.

- [37] Hyunsoo Kim, Haesun Park, and Lars Eldén. Non-negative tensor factorization based on alternating large-scale non-negativity-constrained least squares. In *2007 IEEE 7th International Symposium on BioInformatics and BioEngineering*, pages 1147–1151. IEEE, 2007.
- [38] Jingu Kim and Haesun Park. Fast nonnegative tensor factorization with an active-set-like method. In *High-Performance Scientific Computing*, pages 311–326. Springer, 2012.
- [39] Yangyang Xu and Wotao Yin. A block coordinate descent method for regularized multiconvex optimization with applications to nonnegative tensor factorization and completion. *SIAM Journal on Imaging Sciences*, 6(3):1758–1789, 2013.
- [40] Yong-Deok Kim and Seungjin Choi. Nonnegative Tucker decomposition. In *2007 IEEE Conference on Computer Vision and Pattern Recognition*, pages 1–8. IEEE, 2007.
- [41] Guoxu Zhou, Andrzej Cichocki, and Shengli Xie. Fast nonnegative matrix/tensor factorization based on low-rank approximation. *IEEE Transactions on Signal Processing*, 60(6):2928–2940, 2012.
- [42] Xutao Li, Michael K Ng, Gao Cong, Yunming Ye, and Qingyao Wu. MR-NTD: Manifold regularization nonnegative Tucker decomposition for tensor data dimension reduction and representation. *IEEE Transactions on Neural Networks and Learning Systems*, 28(8):1787–1800, 2016.
- [43] Junjun Pan, Michael K Ng, Ye Liu, Xiongjun Zhang, and Hong Yan. Orthogonal nonnegative tucker decomposition. *arXiv preprint arXiv:1912.06836*, 2019.
- [44] Yuntao Qian, Fengchao Xiong, Shan Zeng, Jun Zhou, and Yuan Yan Tang. Matrix-vector nonnegative tensor factorization for blind unmixing of hyperspectral imagery. *IEEE Transactions on Geoscience and Remote Sensing*, 55(3):1776–1792, 2016.
- [45] J Douglas Carroll and Jih-Jie Chang. Analysis of individual differences in multidimensional scaling via an N-way generalization of “Eckart-Young” decomposition. *Psychometrika*, 35(3):283–319, 1970.
- [46] Richard A Harshman et al. *Foundations of the PARAFAC procedure: Models and conditions for an “explanatory” multimodal factor analysis*. University of California at Los Angeles Los Angeles, CA, 1970.
- [47] Tamara G. Kolda and Brett W. Bader. Tensor decompositions and applications. *SIAM Review*, 51(3):455–500, 2009.
- [48] Lieven De Lathauwer, Bart De Moor, and Joos Vandewalle. A multilinear singular value decomposition. *SIAM Journal on Matrix Analysis and Applications*, 21(4):1253–1278, 2000.
- [49] Ledyard R Tucker. Some mathematical notes on three-mode factor analysis. *Psychometrika*, 31(3):279–311, 1966.
- [50] Guang-Jing Song and Michael K Ng. Nonnegative low rank matrix approximation for nonnegative matrices. *Applied Mathematics Letters*, page 106300, 2020.

- [51] Guang-Jing Song and Michael K Ng. Fast alternating projections on manifolds based on tangent spaces. *arXiv preprint arXiv:2003.10324*, 2020.
- [52] Gene H. Golub and Charles F. Van Loan. *Matrix computations*, volume 3. JHU press, 2012.
- [53] Adrian S. Lewis and Jérôme Malick. Alternating projections on manifolds. *Mathematics of Operations Research*, 33(1):216–234, 2008.
- [54] Adrian S Lewis, David Russel Luke, and Jérôme Malick. Local linear convergence for alternating and averaged nonconvex projections. *Foundations of Computational Mathematics*, 9(4):485–513, 2009.
- [55] Heinz H Bauschke, D Russell Luke, Hung M Phan, and Xianfu Wang. Restricted normal cones and the method of alternating projections: theory. *Set-Valued and Variational Analysis*, 21(3):431–473, 2013.
- [56] Heinz H Bauschke, D Russell Luke, Hung M Phan, and Xianfu Wang. Restricted normal cones and the method of alternating projections: applications. *Set-Valued and Variational Analysis*, 21(3):475–501, 2013.
- [57] Dominikus Noll and Aude Rondepierre. On local convergence of the method of alternating projections. *Foundations of Computational Mathematics*, 16(2):425–455, 2016.
- [58] R. Tyrrell Rockafellar and Roger J.-B. Wets. *Variational analysis*, volume 317. Springer Science & Business Media, 2009.
- [59] F.H. Clarke and R.B. Vinter. Regularity properties of optimal controls. *SIAM Journal on Control and Optimization*, 28(4):980–997, 1990.
- [60] Adrian S. Lewis, D. Russell Luke, and Jérôme Malick. Local linear convergence for alternating and averaged nonconvex projections. *Foundations of Computational Mathematics*, 9(4):485–513, 2009.
- [61] D. Drusvyatskiy, A.D. Ioffe, and A.S. Lewis. Alternating projections and coupling slope. *arXiv preprint arXiv:1401.7569*, pages 1–17, 2014.
- [62] Guoyin Li and Ting Kei Pong. Douglas–rachford splitting for nonconvex optimization with application to nonconvex feasibility problems. *Mathematical Programming*, 159(1-2):371–401, 2016.
- [63] Hedy Attouch, Jérôme Bolte, Patrick Redont, and Antoine Soubeyran. Proximal alternating minimization and projection methods for nonconvex problems: An approach based on the kurdyka-lojasiewicz inequality. *Mathematics of Operations Research*, 35(2):438–457, 2010.
- [64] Zhou Wang, Alan C Bovik, Hamid R Sheikh, and Eero P Simoncelli. Image quality assessment: from error visibility to structural similarity. *IEEE Transactions on Image Processing*, 13(4):600–612, 2004.